Cell

Kynurenine 3-Monooxygenase Inhibition in Blood Ameliorates Neurodegeneration

Daniel Zwilling,[1,9] Shao-Yi Huang,[1,3,9] Korrapati V. Sathyasaikumar,[4] Francesca M. Notarangelo,[4] Paolo Guidetti,[4] Hui-Qiu Wu,[4] Jason Lee,[1] Jennifer Truong,[1] Yaisa Andrews-Zwilling,[1] Eric W. Hsieh,[1] Jamie Y. Louie,[1] Tiffany Wu,[1] Kimberly Scearce-Levie,[1] Christina Patrick,[5] Anthony Adame,[5] Flaviano Giorgini,[6] Saliha Moussaoui,[7] Grit Laue,[7] Arash Rassoulpour,[8] Gunnar Flik,[8] Yadong Huang,[1] Joseph M. Muchowski,[1] Eliezer Masliah,[5] Robert Schwarcz,[4] and Paul J. Muchowski[1,2,3,*]

[1]Gladstone Institute of Neurological Disease
[2]Department of Biochemistry and Biophysics and Department of Neurology
University of California, San Francisco, San Francisco, CA 94158, USA
[3]Taube-Koret Center for Huntington's Disease Research and The Hellman Family Foundation Program in Alzheimer's Disease Research, San Francisco, CA 94158, USA
[4]Maryland Psychiatric Research Center, University of Maryland School of Medicine, Baltimore, MD 21228, USA
[5]Department of Neurosciences, University of California, San Diego, La Jolla, CA 92093, USA
[6]Department of Genetics, University of Leicester, Leicester LE1 7RH, UK
[7]Novartis Institutes for BioMedical Research, CH-4002 Basel, Switzerland
[8]Brains On-Line BV, Antonius Deusinglaan 1, 9713 AV Groningen, The Netherlands
[9]These authors contributed equally to this work
*Correspondence: pmuchowski@gladstone.ucsf.edu
DOI 10.1016/j.cell.2011.05.020

SUMMARY

Metabolites in the kynurenine pathway, generated by tryptophan degradation, are thought to play an important role in neurodegenerative disorders, including Alzheimer's and Huntington's diseases. In these disorders, glutamate receptor-mediated excitotoxicity and free radical formation have been correlated with decreased levels of the neuroprotective metabolite kynurenic acid. Here, we describe the synthesis and characterization of JM6, a small-molecule prodrug inhibitor of kynurenine 3-monooxygenase (KMO). Chronic oral administration of JM6 inhibits KMO in the blood, increasing kynurenic acid levels and reducing extracellular glutamate in the brain. In a transgenic mouse model of Alzheimer's disease, JM6 prevents spatial memory deficits, anxiety-related behavior, and synaptic loss. JM6 also extends life span, prevents synaptic loss, and decreases microglial activation in a mouse model of Huntington's disease. These findings support a critical link between tryptophan metabolism in the blood and neurodegeneration, and they provide a foundation for treatment of neurodegenerative diseases.

INTRODUCTION

Alzheimer's disease (AD) is the most common neurological disease in humans, and Huntington's disease (HD) is among the most common inherited neurodegenerative diseases. The molecular mechanisms of neurodegeneration in these lethal conditions are unclear, and currently no disease-modifying therapies exist.

Experiments in rodents suggest a link between metabolites of the kynurenine pathway (KP), the major route of tryptophan degradation in mammals (Figure 1), and excitotoxicity, a mechanism of neuronal dysfunction and cell death characterized by excessive stimulation of glutamate receptors, pathological elevation of intracellular free calcium, and mitochondrial damage. Many neuropathological features and chemical impairments in HD can be duplicated in experimental animals by an intrastriatal injection of the KP metabolite quinolinic acid (QUIN) (Schwarcz et al., 1983). These findings led to the hypothesis that QUIN, a selective N-methyl-D-aspartate (NMDA) receptor agonist found in mammalian brain, contributes to the pathophysiology of HD.

Excitotoxicity and the KP have also been implicated in the pathogenesis of AD. Injection of QUIN into the nucleus basalis of rats destroys cholinergic neurons projecting to the cortex and causes significant decreases in cortical choline acetyltransferase, acetylcholinesterase, high-affinity choline uptake, and ^{3}H-acetylcholine release, which parallel changes observed in AD brains (Boegman et al., 1985). Continuous intraventricular infusion of QUIN also causes memory deficits that resemble those in AD patients (Misztal et al., 1996).

Kynurenic acid (KYNA), formed in a side arm of the KP (Figure 1), is also thought to modulate excitotoxicity and neurodegeneration. Upon intracerebral application, KYNA blocks QUIN-induced neurodegeneration (Foster et al., 1984), and KYNA is neuroprotective in clinically relevant animal models of brain ischemia (Andiné et al., 1988; Nozaki and Beal, 1992). Notably, genetic reduction in KYNA formation enhances vulnerability to an excitotoxic insult (Sapko et al., 2006). At

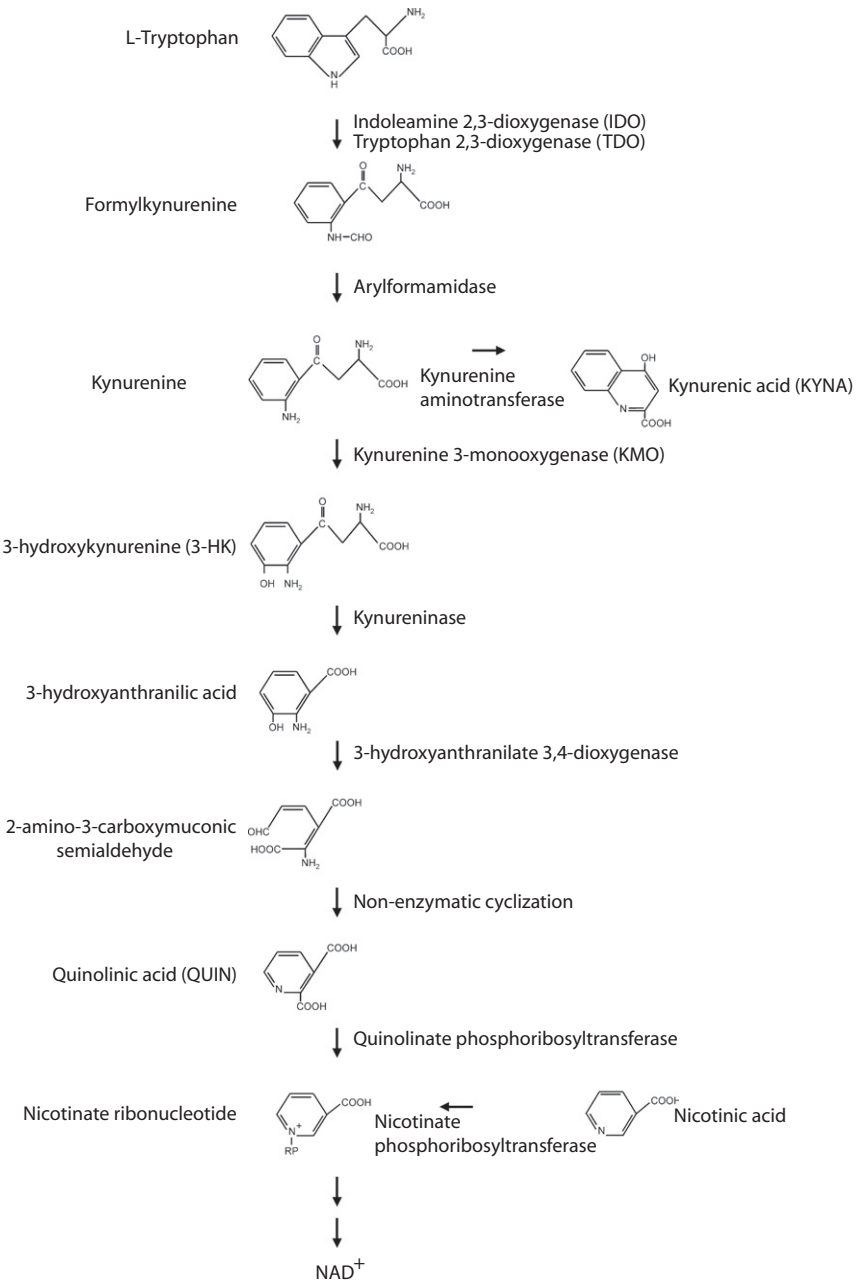

Figure 1. The Kynurenine Pathway of Tryptophan Degradation in Mammals

KMO functions at a key branching point in the kynurenine pathway (KP). Inhibition of KMO causes the accumulation of its substrate kynurenine and a shunt in the KP, leading to increased production of the neuroprotective molecule KYNA.

supraphysiological concentrations, KYNA is a broad-spectrum antagonist of ionotropic excitatory amino acid receptors (Perkins and Stone, 1982). At endogenous brain concentrations, KYNA competitively blocks the glycine coagonist site of the NMDA receptor (Kessler et al., 1989) and noncompetitively inhibits the α7 nicotinic acetylcholine receptor (Hilmas et al., 2001). Even modest increases in brain KYNA reduce extracellular glutamate levels in brain by inhibiting presynaptic α7 nicotinic receptors (Carpenedo et al., 2001).

The neostriatal and neocortical levels of the KP metabolites 3-hydroxykynurenine (3-HK), a free radical generator that mediates neuronal cell death (Okuda et al., 1996), and QUIN are significantly elevated in early pathological-grade HD brains (Guidetti et al., 2004), whereas KYNA levels are decreased (Beal et al., 1992). Moreover, cerebral 3-HK and QUIN concentrations are also increased in mouse models of HD (Guidetti et al., 2006). In the serum of HD patients, tryptophan levels are reduced, and the kynurenine:tryptophan ratio is elevated, coinciding with increased production of proinflammatory cytokines and chemokines (Stoy et al., 2005). Similar findings have been described in AD patients (Gulaj et al., 2010; Heyes et al., 1992a). Thus, analogous changes in KP metabolite levels are found in the central nervous system (CNS) and in the periphery in HD and AD, and it is widely hypothesized that these events are early contributors to the pathophysiology of both diseases.

Kynurenine 3-monooxygenase (KMO) functions at a key branching point of the KP (Figure 1), whereby KMO inhibition shunts KP metabolism toward enhanced KYNA production and may therefore reduce neuronal vulnerability. Indeed, the most widely used KMO inhibitor, Ro 61-8048 (Röver et al., 1997), is beneficial in rodent models of brain ischemia (Moroni et al., 1999), cerebral malaria (Clark et al., 2005), and trypanosomiasis (Rodgers et al., 2009) and in a primate model of Levodopa-induced dyskinesias (Grégoire et al., 2008). However, we found that Ro 61-8048 is metabolically unstable (data not shown) and therefore developed "slow-release" prodrugs of Ro 61-8048 with improved metabolic stability that could be tested in mouse models of chronic neurodegenerative diseases.

Here, we describe the effects of 2-(3,4-dimethoxybenzenesulfonylamino)-4-(3-nitrophenyl)-5-(piperidin-1-yl)methylthiazole (JM6), an orally bioavailable prodrug of Ro 61-8048 (Figure 2A), on behavioral and neuropathological deficits in transgenic mouse models of AD and HD. Treatment with JM6 prevented synaptic loss and behavioral deficits in these models by increasing extracellular brain levels of the neuroprotective KP metabolite KYNA and decreasing extracellular glutamate. We

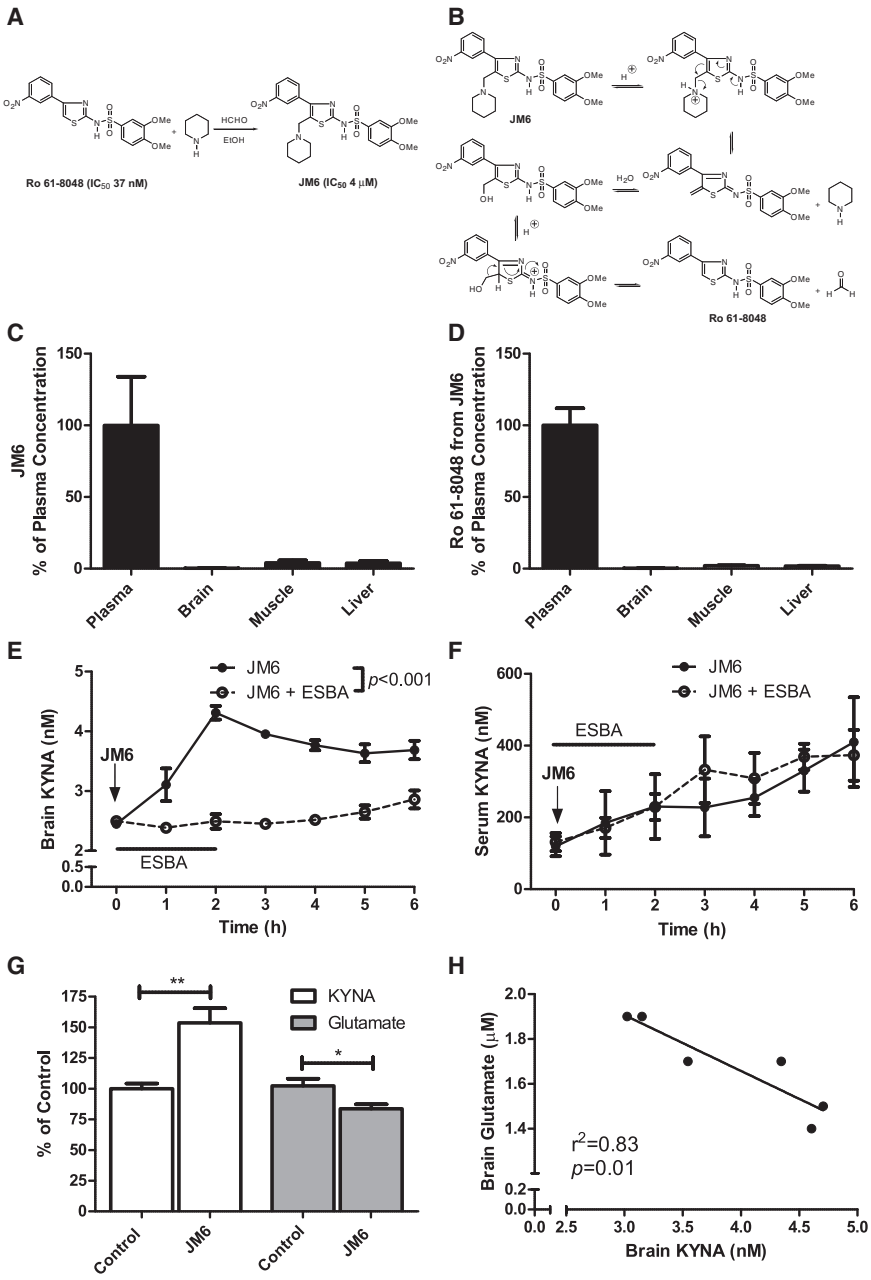

Figure 2. JM6, a Prodrug Inhibitor of KMO, Increases Brain KYNA by Blocking KMO in the Blood

(A) Chemical synthesis of JM6. JM6 is a prodrug of the KMO inhibitor Ro 61-8048.

(B) Hypothetical mechanism for the acid-induced release of Ro 61-8048 from JM6.

(C and D) JM6 (C) and Ro 61-8048 released from JM6 (D) accumulate at high levels in plasma, but not in brain or other tissues, 5 hr after JM6 administration (300 mg/kg p.o.) in mice. Absolute concentrations of JM6 were 40 μM (plasma), 119 nM (brain), 1.6 μM (muscle), and 5 μM (liver) (n = 5). Absolute concentrations of Ro 61-8048 were 7 μM (plasma), 18 nM (brain), 149 nM (muscle), and 132 nM (liver) (n = 5).

(E) Extracellular KYNA levels in the striatum of rats measured by microdialysis following acute JM6 treatment (100 mg/kg, p.o.; arrow). In addition, in one group of animals, the KAT II inhibitor ESBA (1 mM) was applied by reverse dialysis for the first 2 hr and prevented the JM6-induced increase in KYNA levels ($p < 0.001$, repeated measures two-way ANOVA; n = 5 per treatment group).

(F) In the same rats, serum KYNA levels rose equally over time in the two groups, i.e., intracerebral ESBA administration did not influence circulating KYNA levels in JM6-treated rats.

(G) Extracellular KYNA and glutamate were determined by in vivo microdialysis in the prefrontal cortex of rats treated for 7 days with JM6 (100 mg/kg/day p.o.). Baseline values for control rats were 2.5 ± 0.1 nM (KYNA) and 2.0 ± 0.2 μM (glutamate).

(H) Extracellular KYNA correlates negatively with extracellular glutamate in these animals.

*$p < 0.05$; **$p < 0.01$ (t test). n = 6 per group. Values in (C)–(G) are means ± SEM.

found, unexpectedly, that JM6 and Ro 61-8048 do not effectively cross the blood-brain barrier, indicating that peripheral inhibition of KMO is sufficient to confer neuroprotection through the accumulation and active transport of the tryptophan metabolite kynurenine into the brain from the periphery and subsequent conversion to KYNA.

RESULTS

JM6 Increases Brain KYNA by Inhibiting KMO in Blood

We hypothesized that JM6 acts as a prodrug and would be metabolized under acidic conditions in the gut to slowly release Ro 61-8048 and thereby provide long-lasting inhibition of KMO (Figures 2A and 2B). To investigate the pharmacokinetic properties of JM6, we treated wild-type (WT) mice with a single high dose of JM6 (300 mg/kg p.o.) and measured JM6 and Ro 61-8048 in plasma, brain, muscle, and liver by liquid chromatography/mass spectrometry (LC/MS) 5 hr after administration. JM6 accumulated in plasma at a high concentration (39.1 ± 13.2 μM), but only very low levels were detected in the brain (119 ± 46 nM, or 0.003% of plasma levels) (Figure 2C). The brain concentration of JM6 was well below the IC_{50} of this compound for KMO (~4 μM). Ro 61-8048 released from JM6 was also present at a high concentration (7.2 ± 0.8 μM) in plasma but only at very low levels in the brain (18 ± 5 nM, or 0.002% of plasma levels) (Figure 2D), i.e., also below its IC_{50} for KMO (37 nM). Muscle and liver levels of JM6 and Ro 61-8048 after acute dosing were also negligible. Direct administration of Ro 61-8048 (100 mg/kg p.o.) to WT mice also resulted in high

plasma levels but negligible brain exposure (data not shown). Thus, JM6 is a prodrug of Ro 61-8048 in vivo that accumulates predominantly in blood, but neither JM6 itself nor Ro 61-8048 released from JM6 penetrates the blood-brain barrier to any significant extent.

Previous studies have shown that treatment of rodents with Ro 61-8048 raises brain KYNA levels (Röver et al., 1997). However, neither Ro 61-8048 (Figure 2D) nor KYNA (Fukui et al., 1991) crosses the blood-brain barrier effectively. In contrast, the substrate of KMO, kynurenine, is actively transported into the CNS by a neutral amino acid transporter and is then rapidly converted to KYNA (Fukui et al., 1991). We therefore hypothesized that the effect of Ro 61-8048 on brain KYNA levels is secondary to inhibition of KMO in blood cells, followed by an increase in circulating kynurenine levels, active transport of kynurenine into the CNS, and astrocyte-mediated conversion to KYNA.

To test whether systemic administration of JM6 influences the KP in the brain, we performed in vivo microdialysis in the striatum of awake, behaving rats to measure extracellular KYNA as a pharmacodynamic readout of KMO inhibition in the periphery. A single injection of JM6 (100 mg/kg p.o.) increased KYNA levels in both brain (Figure 2E) and serum (Figure 2F), peaking at 180% and 344%, respectively, of baseline levels. JM6 and Ro 61-8048 were detected only at extremely low levels (<10 nM) in brain dialysate (data not shown), similar to results obtained in pharmacokinetic studies (Figures 2C and 2D). In contrast, plasma levels of Ro 61-8048 released from JM6 coincided temporally and were correlated with an increase in KYNA levels in both plasma and brain (data not shown).

In one set of animals, we examined whether the elevation in brain KYNA levels seen after oral administration of JM6 was generated by kynurenine aminotransferase II (KAT II), the enzyme that is predominantly responsible for KYNA production in the rat brain (Guidetti et al., 2007). To this end, rats were treated with JM6 (100 mg/kg p.o.), and a small molecule KAT II inhibitor ([S]-[4-ethylsulfonyl]benzoylalanine hydrochloride; ESBA; Pellicciari et al., 2006) (1 mM) was applied locally for 2 hr by reverse microdialysis. JM6-induced increases in brain KYNA were prevented completely by treatment with ESBA, and KYNA levels in serum were unaffected (Figures 2E and 2F). These results provide unequivocal evidence that increased brain KYNA levels in rats treated with JM6 are due to de novo production of KYNA within the CNS.

Similar increases in extracellular KYNA in the brain were seen in rats treated chronically with JM6 for 7 days (100 mg/kg/day p.o.), and this effect was accompanied by a significant reduction in extracellular glutamate levels (Figure 2G), consistent with a previous microdialysis study in the striatum of rats treated acutely with Ro 61-8048 (4–40 mg/kg i.p.) (Moroni et al., 2005). Importantly, a strong negative correlation between extracellular KYNA and glutamate was observed in rats after treatment with JM6 (Figure 2H). These findings confirm that JM6 is a prodrug that leads to slow release of Ro 61-8048 in blood, increases brain levels of KYNA in a sustained manner by blocking KMO peripherally, and lowers glutamate levels in the brain despite not penetrating the blood-brain barrier.

JM6 Prevents Spatial Memory Loss and Anxiety Deficits in a Mouse Model of AD

Transgenic (tg) mice that overexpress the human amyloid precursor protein (hAPP) are a widely used preclinical model of AD. We next evaluated the effects of JM6 in these APPtg mice, which express hAPP with two familial AD mutations under control of the PDGF promoter ("J20" mice; Mucke et al., 2000). These mutations increase the production of the amyloid β peptide (Aβ), which is widely implicated as a disease-causing agent in AD that forms toxic oligomers and is a component of amyloid plaques, a neuropathological hallmark of AD.

APPtg mice develop spatial memory deficits starting at 4–5 months of age (Chin et al., 2005). JM6 was administered to presymptomatic APPtg mice (75 mg/kg/day p.o.) starting at 2 months of age, and mice were tested behaviorally at ~6 months. Vehicle-treated APPtg mice had significant spatial memory deficits in a Morris water maze assay; however, mutant mice treated with JM6 showed a significant improvement in spatial memory (Figure 3A). JM6 had no effect on spatial memory in WT mice (Figure 3A). Spatial learning was also significantly impaired in APPtg mice, as described (Chin et al., 2005); however, JM6 did not influence learning in WT or APPtg mice (data not shown).

APPtg mice also display deficits in an elevated plus maze (EPM) assay, a measure of anxiety (Chin et al., 2005). In this assay, WT mice spend more time in the closed arm of the maze than in the open arm, whereas APPtg mice spend increased time in the open arm, consistent with disinhibition. Vehicle-treated APPtg mice showed an increase in time spent in the open arm of the maze, but APPtg mice treated with JM6 were not significantly different from WT littermate controls (Figure 3B). The distance traveled in the open arm was significantly increased in APPtg mice, and this increase was significantly attenuated in APPtg mice that received JM6 (Figure 3C). The total distance traveled in the EPM (open and closed arm) was also significantly increased in APPtg mice, but this phenotype was not changed in APPtg mice that received JM6 (Figure 3D).

JM6 Prevents Synaptic Loss in a Mouse Model of AD

Synaptic loss in APPtg mice correlates with spatial memory loss (Mucke et al., 2000) and may be an important contributor to pathogenesis in AD patients (Masliah et al., 1989). Consistent with past studies (Chin et al., 2005), APPtg mice had reduced levels of synaptophysin in the cortex and hippocampus at ~7 months of age (Figures 4A–4D). Synaptic loss was prevented in APPtg mice treated with JM6. However, JM6 did not have a significant effect on Aβ plaque load, which was increased in the hippocampus and cortex in APPtg mice (data not shown).

JM6 Increases Brain KYNA Levels in a Mouse Model of AD

In the serum and CSF of AD patients, tryptophan levels are reduced and the kynurenine:tryptophan ratio is elevated, coinciding with increased production of proinflammatory cytokines and chemokines (Gulaj et al., 2010; Heyes et al., 1992a). APPtg mice had lower brain KYNA levels than WT littermate controls (Figure 5A). Chronic treatment of APPtg mice with JM6 (75 mg/kg/day p.o. for 120 days) increased brain and

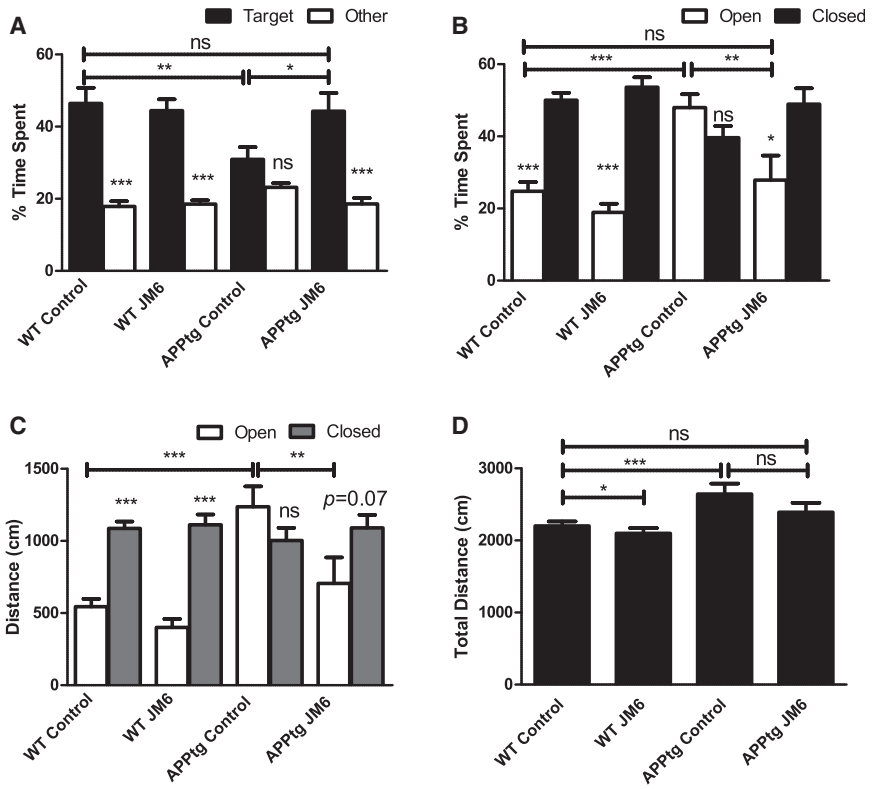

Figure 3. JM6 Prevents Spatial Memory Loss and Anxiety Deficits in a Mouse Model of AD

(A) JM6 rescues spatial memory deficits in APPtg mice in the Morris water maze (MWM). Mice were trained to find a hidden platform in the MWM using spatial cues. Spatial memory was assessed 24 hr after training by removing the hidden platform and quantifying how much time mice spent in the target quadrant where the platform had been placed previously. APPtg mice that received JM6 (75 mg/kg/day p.o. for 120 days starting at day 30) spend significantly more time in the target quadrant than vehicle-treated controls. Solid bar, target quadrant; white bar, average of three other quadrants.

(B) JM6 reduces anxiolytic behavior in APPtg mice in the elevated plus maze (EPM). APPtg mice are disinhibited and spend an equal amount of time in the open and closed arms in the EPM. However, APPtg mice that receive JM6 spend significantly more time in the closed arm than in the open arm and are not significantly different from WT mice. Values are means ± SEM. *$p < 0.05$, **$p < 0.01$, ***$p < 0.001$.

(A and B) For (A) and (B), t tests were used to calculate differences between target versus other quadrants and time spent in open versus closed arm, respectively (n = 8–14 mice per group). One-way ANOVA was used to calculate differences among the four experimental groups. JM6 reduces the distance traveled by APPtg mice in the open arm of the elevated plus maze.

(C and D) APPtg mice that receive JM6 travel significantly less distance in the open arm of the EPM than vehicle-treated controls, but the total travel distance in both arms of the maze is not different. Values are means ± SEM.

***$p < 0.001$ (t test, open versus closed arm); **$p < 0.01$; ***$p < 0.001$ (one-way ANOVA comparing open arms between groups). n = 8–14 per group. ns, not significant.

plasma levels of KYNA (Figures 5A and 5B). Notably, KMO activity, 3-HK and QUIN levels in the brains of APPtg mice treated with JM6, and QUIN levels in plasma were not significantly different than in control mice (Figures 5C–5F).

JM6 Increases Survival in a Mouse Model of HD

We next evaluated the effects of JM6 in R6/2 mice, the best characterized and most widely used genetic model of HD. In these mice, the first exon of the huntingtin gene (*IT-15*) with a large CAG repeat expansion is expressed under the control of the 5′ end of human *IT-15* (Mangiarini et al., 1996). R6/2 mice reliably develop progressive neurological phenotypes, including motor deficits, weight loss, and premature death. These features, along with the rapid progression of symptoms and the relatively short life span of the mice, have contributed to their popularity and utility for preclinical studies.

When administered starting at 4 weeks of age, an early symptomatic stage in these mice, JM6 (7.5 or 25 mg/kg/day p.o.) had a highly significant, dose-dependent effect on survival (Figure 6A), as shown by Kaplan-Meier survival analysis. In a separate cohort of R6/2 mice that received behavioral enrichment, which can increase survival of R6/2 mice (Hockly et al., 2002), JM6 had a similar effect on survival (Figure 6B). JM6 did not influence body weight but modestly improved performance on an accelerating rotarod at early stages of disease (data not shown). Treatment of WT mice with JM6 for 12 months (25 mg/kg/day p.o.) had no adverse effects on open field behavior, motor performance, or body weight (data not shown).

JM6 Prevents Synaptic Loss and CNS Inflammation in a Mouse Model of HD

R6/2 mice are characterized by loss of the presynaptic marker synaptophysin in the cortex and striatum by 11–15 weeks (Cepeda et al., 2003; Wacker et al., 2009). JM6 (7.5 or 25 mg/kg/day p.o.) prevented the loss of synaptophysin in the striatum (Figures 6C and 6D) and cortex (data not shown) of 12-week-old R6/2 mice. JM6 also prevented the loss of immunoreactivity of Fos, a calcium-regulated immediate-early gene product that is a surrogate marker for neuronal activity and is decreased (Wacker et al., 2009) in the striatum (Figures 6E and 6F) and cortex (data not shown) of 12-week-old R6/2 mice. These results suggest that JM6 preserves synapses and also may stabilize synaptic activity in R6/2 mice. Previous studies in R6/2 mice and HD brains showed increased staining with an antibody to the protein Iba1 (Simmons et al., 2007; Wacker et al., 2009), consistent with microglial activation and/or proliferation. R6/2 mice treated with JM6 had significantly fewer Iba1-positive cells than vehicle-treated controls (Figures 6G and 6H) and were not

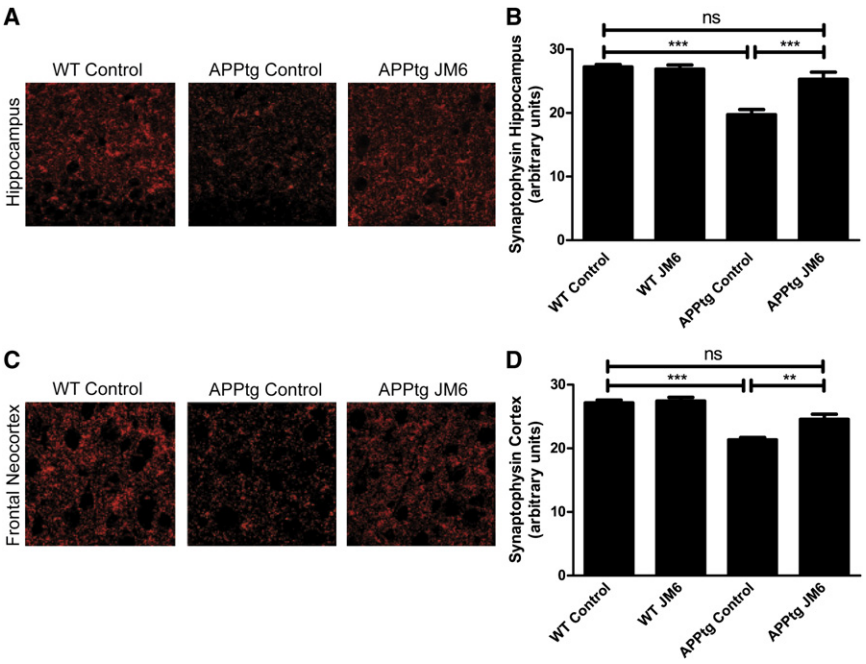

Figure 4. JM6 Prevents Synaptic Loss in a Mouse Model of AD

(A–D) JM6 (75 mg/kg/day p.o. for 120 days starting at day 30) prevents synaptic loss in the hippocampus and cortex of ~7 month-old APPtg mice. (A and C) Representative images (630X) of serial sections of the hippocampus (A) and frontal cortex (C) of WT or APPtg mice immunostained with an antibody for synaptophysin.

(B and D) Quantification of synaptophysin levels in the hippocampus (B) and frontal cortex (D) of APPtg mice treated with JM6. Synaptophysin levels in APPtg mice treated with JM6 are not significantly (ns) different than those found in WT mice.

Values are means ± SEM. **$p < 0.01$; ***$p < 0.001$ (one-way ANOVA). n = 5–9 per group.

significantly different than WT littermate controls, suggesting that microglial activation was prevented in the brains of these mice.

R6/2 mice also display neuronal inclusion bodies (Scherzinger et al., 1997), a pathological hallmark of HD and other polyglutamine diseases (DiFiglia et al., 1997). Immunohistochemical experiments on brain sections from the frontoparietal cortex of R6/2 mice treated chronically with JM6 indicated that JM6 did not influence inclusion body size (data not shown) or abundance (Figures 6I and 6J).

Consistent with acute studies in rats (Figures 2C and 2D), Ro 61-8048 released from JM6 accumulated in plasma from chronically treated R6/2 mice at a concentration of ~280 nM, i.e., > 8-fold higher than its IC_{50} for KMO (37 nM), but could not be detected in brain or muscle homogenates (data not shown).

DISCUSSION

This study shows that prolonged oral administration of JM6, a novel prodrug inhibitor of KMO, ameliorates neurodegeneration in well-established genetic mouse models of AD and HD. Inhibition of KMO by JM6-derived Ro 61-8048 in the blood prevented behavioral deficits, synaptic loss, and other markers of neurodegeneration, even though neither the prodrug nor its metabolite, which directly inhibits KMO, crosses the blood-brain barrier into the CNS. Our findings demonstrate that peripheral inhibition of KMO raises brain levels of the neuroprotective KP metabolite KYNA while decreasing glutamate release in a sustained manner. Because KMO is expressed at high levels in peripheral immune cells such as macrophages (Heyes et al., 1992b), our findings suggest that KMO and its effects on tryptophan metabolism in the KP constitute a critical mediator between the peripheral immune system and excitotoxic processes in the CNS.

Consistent with a neuroprotective role for KYNA, prolonged peripheral administration of relatively large doses of the KMO substrate kynurenine (which leads to increased brain KYNA) rescues behavioral and neuropathological deficits in acute models of neurodegeneration (Carrillo-Mora et al., 2010; Silva-Adaya et al., 2010). However, peripheral inhibition of KMO using the prodrug methodology described here may be a safer and more attractive therapeutic approach because it involves modest and sustained elevations in brain KYNA levels *without* increasing 3-HK and QUIN levels in the blood and brain. This will avoid potential adverse consequences both within the brain and on peripheral immune system function.

Our findings suggest that JM6 is neuroprotective by raising CNS levels of KYNA and by decreasing glutamate levels and thus excitotoxicity mediated by glutamate receptors (Figure 7). Interestingly, other studies implicate deficient glutamate uptake in HD (Liévens et al., 2001) and AD (Masliah et al., 1996), and increased expression of the glutamate transporter GLT1 is neuroprotective in a mouse model of HD (Miller et al., 2008). Notably, because JM6 does not increase CNS KYNA levels sufficiently to block glutamate receptors directly, it is likely that decreased extracellular glutamate observed after JM6 treatment is caused secondarily following KYNA antagonism of α7 nicotinic acetylcholine receptors (Hilmas et al., 2001). Consistent with this scenario, deletion of the α7 nicotinic acetylcholine receptor gene improves cognitive deficits and synaptic pathology in a mouse model of AD (Dziewczapolski et al., 2009).

Neuroprotection by KYNA may also be due, in part, to its ability to regulate innate and adaptive immune responses (Romani et al., 2008). For example, KYNA is an agonist of GPR35, an orphan G protein-coupled receptor that reduces production of the proinflammatory cytokine TNF-α (Wang et al., 2006), which is found at abnormally high levels in patients with HD (Björkqvist et al., 2008) and AD (Fillit et al., 1991). Inhibition of TNF-α signaling is neuroprotective in mouse models of AD (Yamamoto et al., 2007). Although we did not directly measure levels of

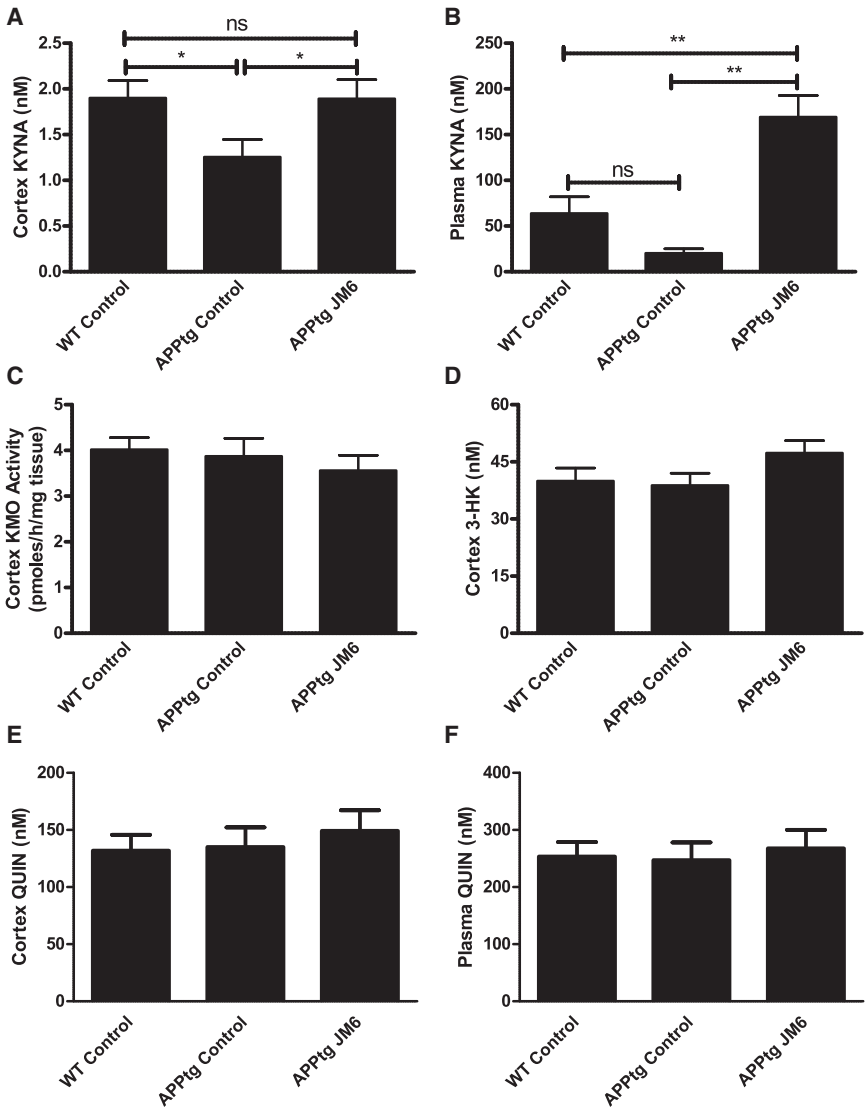

Figure 5. JM6 Increases Brain KYNA Levels in a Mouse Model of AD

(A) Compared to WT mice, cortical KYNA levels are significantly reduced in APPtg mice, and the deficit is normalized by JM6 treatment (75 mg/kg/day p.o. for 120 days starting at day 30).

(B) Plasma KYNA measurements in the same three groups show a similar pattern as in the brain.

(C–F) No group differences are seen in cortical KMO activity (C), 3-HK levels (D), and QUIN levels (E), as well as in plasma QUIN levels (F).

Values are means ± SEM. n = 5–15 per group, except APPtg controls in (B), for which n = 3. *$p < 0.05$; **$p < 0.01$ (t test). ns, not significant.

TNF-α and other proinflammatory cytokines in our studies, treatment of R6/2 mice with JM6 normalized levels of a protein marker for microglia, suggesting a decrease in the inflammatory environment in the CNS of these mice. Future studies will be required to elucidate fully how JM6 and KMO modulate the immune system in mouse models of neurodegeneration.

A recent complementary study provides compelling genetic and pharmacological evidence that KMO modulates neurodegeneration in a fruit fly model of HD (Campesan et al., 2011) and that an increased KYNA:3-HK ratio provides neuroprotection. Genetic dissection in the flies indicated that KP enzymes other than KMO might also be attractive therapeutic targets for HD and other neurodegenerative diseases. Notably, the experiments described by Campesan et al. and in our current study stemmed, in part, from the identification of KMO in a yeast genetic screen designed to isolate suppressors of mutant huntingtin toxicity (Giorgini et al., 2005). Interestingly, genetic or pharmacological inhibition of KMO suppressed mutant huntingtin toxicity in yeast, despite the absence of genes that encode neurotransmitter receptors and immune signaling molecules in the yeast genome. However, mutant huntingtin toxicity in yeast was tightly correlated to increased levels of 3-HK, QUIN, and reactive oxygen species (Giorgini et al., 2005). As KMO is an outer mitochondrial membrane protein, these results suggest that KMO and KP metabolites may also influence neurodegenerative processes by modulating mitochondrial function. Thus, our results provide additional evidence that genetic screens in model organisms can successfully identify disease-modifying pathways that are conserved in lower and higher eukaryotes.

In summary, because neurodegenerative disorders such as AD and HD are characterized by increased levels of toxic KP metabolites and decreased levels of KYNA, a rational strategy for treating these disorders may be to normalize brain levels of KYNA by inhibiting KMO in blood cells. KYNA may be beneficial in these diseases due to its ability to modulate neurotransmission, immune cell function, and mitochondrial function in a manner that contributes to neuroprotection.

EXPERIMENTAL PROCEDURES

Synthesis of 2-(3,4-Dimethoxybenzenesulfonylamino)-4-(3-Nitrophenyl)-5-(Piperidin-1-yl)Methylthiazole

To a stirred solution of Ro 61-8048 (structure in Figure 2) in ethanol was added 10 molar equivalents of aqueous formaldehyde (37 WT %) and an equimolar amount of the amine. After 0.5 hr, the precipitated solid was collected by filtration, washed successively with water and ethanol, and dried in vacuo to generate JM6. JM6 (structure in Figure 2) was obtained in 88% yield and had a melting point of 193°C –194°C. ^{1}H NMR (DMSO d_6) δ 1.39 (bs, 2H), 1.52 (bs, 4H), 2.45 (bs, 4H), 3.55 (bs, 2H), 3.79 (s, 3H), 3.83 (s, 3H), 7.07 (d, 1H, J = 8.4 Hz), 7.30 (d, 1H, J = 2.0 Hz), 7.39 (dd, 1H, J = 8.4, 2.0 Hz), 7.74 (t, 1H,), 7.93 (d, 1H, J = 8.0 Hz), 8.25 (dd, 1H, J = 8.4, 1.6 Hz), 8.43 (s, 1H), 12.41 (bs, 1H); MS-ESI m/z 519 $(MH)^+$.

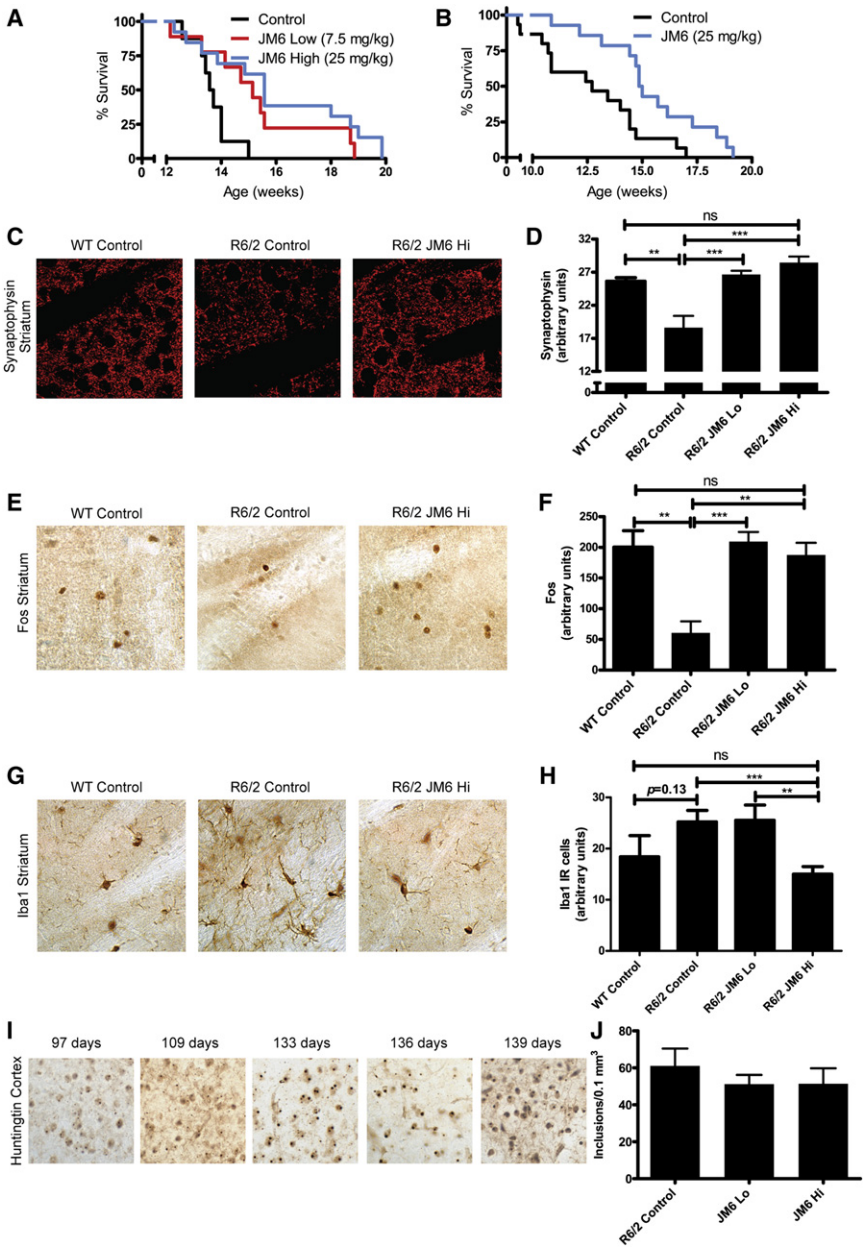

Figure 6. JM6 Prevents Neurodegeneration in a Mouse Model of HD

(A) Kaplan-Meier survival analysis shows that chronic JM6 administration (7.5 or 25 mg/kg/day p.o., starting at 4 weeks of age) increases survival in R6/2 mice in the absence of behavioral enrichment. Log rank; $p = 0.017$; $n = 8–13$ per group.

(B) Kaplan-Meier survival analysis shows that chronic JM6 administration (25 mg/kg/day p.o. starting at 4 weeks of age) increases survival in an independent cohort of R6/2 that received behavioral enrichment. Log rank; $p = 0.005$; $n = 14–15$ per group.

(C and D) JM6 (7.5 or 25 mg/kg/day p.o., starting at 4 weeks of age) prevents synaptic loss in R6/2 mice. (C) Representative images (630×) of serial sections of striatum from WT or R6/2 mice immunostained with an antibody for synaptophysin. (D) Quantification of synaptophysin levels in R6/2 mice treated with JM6.

(E and F) JM6 (7.5 or 25 mg/kg/day p.o., starting at 4 weeks of age) prevents the loss of Fos, a marker for neuronal activity, in R6/2 mice. (E) Representative images (440×) of serial sections of the striatum from WT or R6/2 mice immunostained with an antibody for Fos. (F) Quantification of Fos levels in R6/2 mice treated with JM6.

(G and H) JM6 (7.5 or 25 mg/kg/day p.o., starting at 4 weeks of age) decreases CNS inflammation in R6/2 mice. (G) Representative images (440×) of serial sections of the striatum from WT or R6/2 mice immunostained with an antibody against Iba1 that labels microglia. (H) Iba1 levels in R6/2 mice treated with JM6 (7.5 or 25 mg/kg/day p.o., starting at 4 weeks of age). Levels of synaptophysin, Fos, and Iba1 in R6/2 mice treated with JM6 are not significantly different than those in WT mice.

(I) Brain sections from the cortex of 97- to 139-day-old R6/2 mice that received JM6 (25 mg/kg/day p.o., starting at 4 weeks of age) were immunostained with an anti-huntingtin antibody (EM48). Inclusion bodies increase in size and abundance between 97 and 139 days of age.

(J) In the same animals, JM6 does not significantly decrease the abundance of inclusion bodies, as determined by quantification of EM48 immunostaining.

Values are means ± SEM. $^{**}p < 0.01$; $^{***}p < 0.001$ (one-way ANOVA). $n = 5–13$ per group. ns, not significant.

Animals and Behavioral Testing

All animals were housed and handled in accordance with the National Institutes of Health "Guide for the Care and Use of Laboratory Animals." All studies were approved by the Institutional Animal Care and Use Committee of the University of California, San Francisco (mice) or the University of Maryland, Baltimore (rats). All animals were housed in pathogen-free barrier facilities on a 12 hr light/dark cycle. Male and female R6/2 mice used in the study with 113 ± 0.5 CAG repeats were generated from the sixth generation backcross of male R6/2 breeders to C57BL/6 females. CAG sizing was performed by PCR amplification with a labeled primer using an ABI3730 with genemapper software (Laragen, Culver City, CA). APPtg mice were maintained on a C57BL/6 background (Harris et al., 2010). Mice were genotyped using DNA from tail snips and group housed with access to water and food ad libitum. Behavioral testing occurred between 8 AM and 5 PM during the light cycle, except where noted. Experimenters were blind to mouse genotype and treatment during testing. Survival in R6/2 mice was evaluated as the time when the animals either died spontaneously or had lost more than 20% of their maximal weight. APPtg mice were tested using the Morris water maze and EPM at 7 months of age, as described (Harris et al., 2010).

Acute and Chronic Administration of JM6

For all acute studies, JM6 was administered as a sonicated suspension in 0.1% Tween-80 in water by oral gavage. For chronic administration, JM6 was weighed and mixed with powdered chow (Lab Diet, Richmond, IN) in a blender. A single glass feeding jar (Dyets, Bethlehem, PA) that contained powdered chow (with and without treatment) was placed in each cage and refilled as necessary. Feeders were monitored each day, and body weight was determined twice per week.

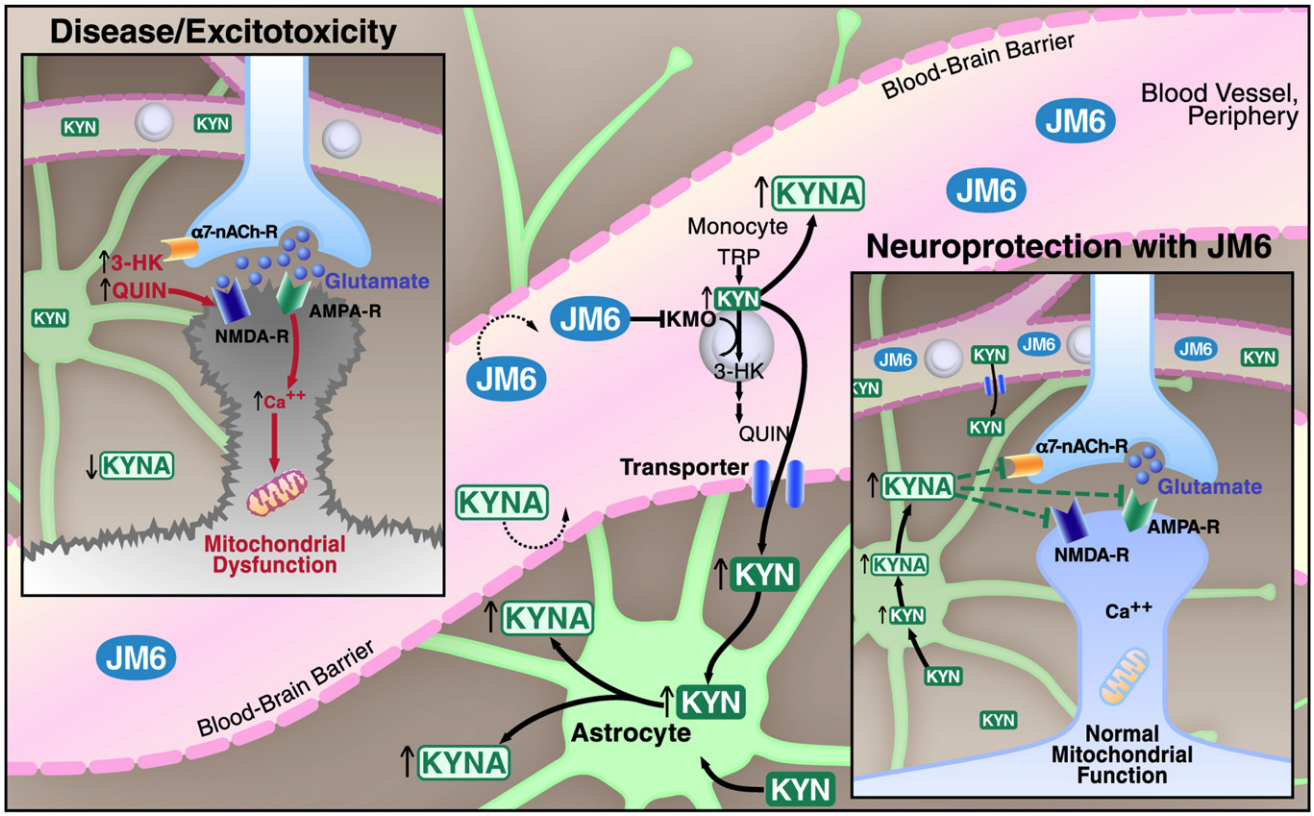

Figure 7. A Model Illustrating the Mechanism by Which KMO Inhibition in Blood Cells Leads to Elevated Brain KYNA Levels and Neuroprotection

In neurodegenerative diseases like HD and AD, increased levels of the toxic kynurenine pathway metabolites 3-HK and QUIN and decreased levels of the neuroprotective pathway metabolite KYNA might contribute to increased glutamatergic neurotransmission, elevation of intracellular calcium levels, mitochondrial dysfunction, and ultimately neuronal dysfunction and cell death (inset labeled "Disease/Excitotoxicity"). We hypothesize that the biotransformation of JM6 to Ro 61-8048 in the gut (not shown) results in KMO inhibition in peripheral monocytes, causing the accumulation of both kynurenine (KYN) and KYNA in blood. Unlike KYNA, KYN is then actively transported into the brain, where it is rapidly converted by astrocytes to KYNA. KYNA released from astrocytes mediates neuroprotection, at least in part, by decreasing glutamate levels via antagonism of presynaptic α7 nicotinic acetylcholine receptors (inset labeled "Neuroprotection with JM6"). However, at high local concentrations, KYNA might also directly block glutamate receptors to reduce excitotoxicity. Neuroprotection by JM6 might also involve a decrease in inflammation and modulation of mitochondrial function (not shown).

In Vivo Brain Microdialysis and Blood Sample Collection

Male Sprague-Dawley rats (280–350 g) were anesthetized with chloral hydrate (360 mg/kg i.p.) and placed in a David Kopf stereotaxic frame. A guide cannula (outer diameter 0.65 mm) was positioned over the striatum (AP, 1 mm anterior to bregma; L, 2.5 mm from midline; V, 3.5 mm below the dura) and secured to the skull with acrylic dental cement and anchor screws. On the next day, a microdialysis probe (CMA/10, membrane length: 2–4 mm, Carnegie Medicin, Stockholm, Sweden) was inserted through the guide cannula and connected to a microperfusion pump set to a speed of 1 μl/min. The freely moving animals were perfused with Ringer solution containing (in mM): NaCl, 144; KCl, 4.8; $MgSO_4$, 1.2; $CaCl_2$, 1.7; pH 6.7. Where indicated, ESBA (kindly provided by R. Pellicciari, Univ. Perugia, Italy) was applied by reverse dialysis for 2 hr. Subsequently, perfusion with Ringer solution continued. Microdialysis samples were collected every 30 or 60 min for the duration of the experiment. To obtain blood samples, rats received a jugular vein catheter (polyethylene tubing, 0.58 mm inner diameter) during anesthesia for the guide cannula implantation described above. The catheter was kept patent by filling it with a 5 mM EDTA solution to prevent coagulation. On the next day, blood (500 μl) was withdrawn hourly during ongoing microdialysis.

Essentially identical methods were used to obtain brain microdialysis and blood samples, respectively, for the measurement of JM6 and Ro 61-8048 in separate rats.

Analysis of KP Metabolites, Glutamate, JM6, and Ro 61-8048

Tissues were sonicated (1:5, wt/vol) in ultrapure water. Twenty five μl of 6% perchloric acid were added to 100 μl of the homogenate, and the suspension was thoroughly mixed and centrifuged (16,000 × g for 15 min). Twenty μl of the supernatant were subjected to HPLC analysis. KYNA was determined fluorimetrically (excitation, 344 nm; emission, 398 nm), and 3-HK was measured electrochemically (oxidation potential: +0.5 V) (modified from Guidetti et al., 2006).

For the determination of serum KYNA levels (Figure 2F), venous blood was allowed to clot (15 min) and was then centrifuged (microfuge). For KYNA measurement in plasma (Figure 5B), blood was collected in EDTA-containing tubes and centrifuged (microfuge). Both preparations were diluted (1:10, vol/vol) and deproteinated (25 μl of 6% perchlorate added to 100 μl; see above), and 20 μl of the respective supernatant were subjected to HPLC analysis.

KYNA and glutamate levels in microdialysate samples were determined as described previously (Rassoulpour et al., 2005). QUIN was quantified by

GC/MS in the same tissue or plasma used for the determination of KYNA. Analyses were performed on a 7890A GC coupled to a 7000 MS/MS (Agilent Technologies, Santa Clara, CA), using an adaptation of the method described by Eckstein et al. (2008). The concentrations of JM6 and Ro 61-8048 were determined by LC/MS in appropriate microdialysate, plasma, and tissue samples.

Measurement of KMO Activity

Brain tissue was homogenized 1:5 (wt/vol) in ultrapure water and further diluted 1:5 (vol/vol) in 100 mM Tris-HCl buffer (pH 8.1) containing 10 mM KCl and 1 mM EDTA. Eighty μl of the tissue preparation were incubated for 40 min at 37°C in a solution containing 1 mM NADPH, 3 mM glucose-6-phosphate, 1 U/ml glucose-6 phosphate dehydrogenase, 100 μM kynurenine, 10 mM KCl, and 1 mM EDTA in a total volume of 200 μl. The reaction was stopped by the addition of 50 μl of 6% perchloric acid. Blanks were obtained by adding the specific enzyme inhibitor Ro 61-8048 (100 μM) in the incubation solution. After centrifugation (16,000 × g, 15 min), 20 μl of the supernatant were applied to HPLC to measure 3-HK (see above).

Neuropathological Analyses

The right hemibrain was immersion-fixed in 4% paraformaldehyde in phosphate-buffered saline (PBS) (pH 7.4) and serially sectioned at 40 μm with a microtome (Vibratome, Leica, Deerfield, IL) for neuropathological analysis, as described (Harris et al., 2010). To investigate the effects of JM6 on levels of mutant huntingtin immunoreactivity in R6/2 mutant mice, the sections were immunolabeled overnight with a rabbit polyclonal antibody (EM48, Chemicon) against a glutathione S transferase fusion protein containing the first 256 amino acids of huntingtin lacking the polyQ and polyproline stretches. Sections were washed in PBS and placed in biotinylated secondary antibody (1:100) (Vector Laboratories, Burlingame, CA) for 2 hr. Sections were placed in 20% diaminobenzidene (DAB) (Vector Laboratories), mounted, dried, and coverslipped with Entillin (Fisher). Three immunostained sections per mouse were imaged with an Olympus digital microscope. A total of 10 digital images per section and region of interest were analyzed with Image-Pro Plus to determine the optical density per field and the mean diameter and number of intranuclear inclusions. Individual values were averaged and expressed as mean value. To investigate the effects of JM6 on microglial activation, microtome sections from R6/2 mice were immunostained with a mouse monoclonal antibody against Iba-1 (microglial cell marker, 1:1000, DakoCytomation, Carpinteria, CA) followed by biotinylated secondary antibody, avidin coupled to horseradish peroxidase, and reacted with DAB, as described (Harris et al., 2010). Sections were analyzed, and the numbers of Iba-1-positive microglia were averaged and expressed as total number per 0.1 mm^3. To determine the number of microglia per unit area, 10 digital images per field were obtained and analyzed with Image-Pro Plus. From each case, at least three blind-coded random sections were analyzed, and the results were averaged and expressed as mean value. To investigate the effect of JM6 on plaque load in APPtg mice, microtome sections were immunostained with a biotinylated monoclonal mouse antibody 3D6 (Elan Pharmaceuticals) against amyloid β peptide followed by avidin coupled to horseradish peroxidase and reacted with DAB as described (Harris et al., 2010). Images of hippocampus and cortex were obtained with a Leica DM5000 B microscope, and the percent area covered by 3D6 immunoreactive material was analyzed with Image J, version 1.43u. Two sections were analyzed per mouse.

ACKNOWLEDGMENTS

This study was supported by the J. David Gladstone Institutes (P.J.M.), National Institutes of Health grants AG022074 (P.J.M., Y.H., and E.M.) and NS057715 (P.J.M. and R.S.), the Taube-Koret Center for Huntington's Disease Research and the Hellman Family Foundation Program in Alzheimer's Disease Research (P.J.M.), and a postdoctoral fellowship from the American Health Assistance Foundation (D.Z.). The J. David Gladstone Institutes received support from a National Center for Research Resources Grant RR18928-01. The authors thank S. Ordway and G. Howard for editorial assistance and S. Finkbeiner for helpful discussions. This study is dedicated in loving memory to Dr. Paolo Guidetti (June 5, 1966–December 28, 2007), who tragically passed away during the course of this study after a battle with cancer.

Received: January 18, 2011
Revised: April 30, 2011
Accepted: May 12, 2011
Published online: June 2, 2011

REFERENCES

Andiné, P., Lehmann, A., Ellrén, K., Wennberg, E., Kjellmer, I., Nielsen, T., and Hagberg, H. (1988). The excitatory amino acid antagonist kynurenic acid administered after hypoxic-ischemia in neonatal rats offers neuroprotection. Neurosci. Lett. *90*, 208–212.

Beal, M.F., Matson, W.R., Storey, E., Milbury, P., Ryan, E.A., Ogawa, T., and Bird, E.D. (1992). Kynurenic acid concentrations are reduced in Huntington's disease cerebral cortex. J. Neurol. Sci. *108*, 80–87.

Björkqvist, M., Wild, E.J., Thiele, J., Silvestroni, A., Andre, R., Lahiri, N., Raibon, E., Lee, R.V., Benn, C.L., Soulet, D., et al. (2008). A novel pathogenic pathway of immune activation detectable before clinical onset in Huntington's disease. J. Exp. Med. *205*, 1869–1877.

Boegman, R.J., el-Defrawy, S.R., Jhamandas, K., Beninger, R.J., and Ludwin, S.K. (1985). Quinolinic acid neurotoxicity in the nucleus basalis antagonized by kynurenic acid. Neurobiol. Aging *6*, 331–336.

Campesan, S., Green, E.W., Breda, C., Sathyasaikumar, K.V., Muchowski, P.J., Schwarcz, R., Kyriacou, C.P., and Giorgini, F. (2011). The kynurenine pathway modulates neurodegeneration in a Drosophila model of Huntington's disease. Curr. Biol. *21*, 961–966.

Carpenedo, R., Pittaluga, A., Cozzi, A., Attucci, S., Galli, A., Raiteri, M., and Moroni, F. (2001). Presynaptic kynurenate-sensitive receptors inhibit glutamate release. Eur. J. Neurosci. *13*, 2141–2147.

Carrillo-Mora, P., Méndez-Cuesta, L.A., Pérez-De La Cruz, V., Fortoul-van Der Goes, T.I., and Santamaría, A. (2010). Protective effect of systemic L-kynurenine and probenecid administration on behavioural and morphological alterations induced by toxic soluble amyloid beta (25-35) in rat hippocampus. Behav. Brain Res. *210*, 240–250.

Cepeda, C., Hurst, R.S., Calvert, C.R., Hernández-Echeagaray, E., Nguyen, O.K., Jocoy, E., Christian, L.J., Ariano, M.A., and Levine, M.S. (2003). Transient and progressive electrophysiological alterations in the corticostriatal pathway in a mouse model of Huntington's disease. J. Neurosci. *23*, 961–969.

Chin, J., Palop, J.J., Puoliväli, J., Massaro, C., Bien-Ly, N., Gerstein, H., Scearce-Levie, K., Masliah, E., and Mucke, L. (2005). Fyn kinase induces synaptic and cognitive impairments in a transgenic mouse model of Alzheimer's disease. J. Neurosci. *25*, 9694–9703.

Clark, C.J., Mackay, G.M., Smythe, G.A., Bustamante, S., Stone, T.W., and Phillips, R.S. (2005). Prolonged survival of a murine model of cerebral malaria by kynurenine pathway inhibition. Infect. Immun. *73*, 5249–5251.

DiFiglia, M., Sapp, E., Chase, K.O., Davies, S.W., Bates, G.P., Vonsattel, J.P., and Aronin, N. (1997). Aggregation of huntingtin in neuronal intranuclear inclusions and dystrophic neurites in brain. Science *277*, 1990–1993.

Dziewczapolski, G., Glogowski, C.M., Masliah, E., and Heinemann, S.F. (2009). Deletion of the alpha 7 nicotinic acetylcholine receptor gene improves cognitive deficits and synaptic pathology in a mouse model of Alzheimer's disease. J. Neurosci. *29*, 8805–8815.

Eckstein, J.A., Ammerman, G.M., Reveles, J.M., and Ackermann, B.L. (2008). Simultaneous profiling of multiple neurochemical pathways from a single cerebrospinal fluid sample using GC/MS/MS with electron capture detection. J. Mass Spectrom. *43*, 782–790.

Fillit, H., Ding, W.H., Buee, L., Kalman, J., Altstiel, L., Lawlor, B., and Wolf-Klein, G. (1991). Elevated circulating tumor necrosis factor levels in Alzheimer's disease. Neurosci. Lett. *129*, 318–320.

Foster, A.C., Vezzani, A., French, E.D., and Schwarcz, R. (1984). Kynurenic acid blocks neurotoxicity and seizures induced in rats by the related brain metabolite quinolinic acid. Neurosci. Lett. *48*, 273–278.

Fukui, S., Schwarcz, R., Rapoport, S.I., Takada, Y., and Smith, Q.R. (1991). Blood-brain barrier transport of kynurenines: implications for brain synthesis and metabolism. J. Neurochem. *56*, 2007–2017.

Giorgini, F., Guidetti, P., Nguyen, Q., Bennett, S.C., and Muchowski, P.J. (2005). A genomic screen in yeast implicates kynurenine 3-monooxygenase as a therapeutic target for Huntington disease. Nat. Genet. *37*, 526–531.

Grégoire, L., Rassoulpour, A., Guidetti, P., Samadi, P., Bédard, P.J., Izzo, E., Schwarcz, R., and Di Paolo, T. (2008). Prolonged kynurenine 3-hydroxylase inhibition reduces development of levodopa-induced dyskinesias in parkinsonian monkeys. Behav. Brain Res. *186*, 161–167.

Guidetti, P., Luthi-Carter, R.E., Augood, S.J., and Schwarcz, R. (2004). Neostriatal and cortical quinolinate levels are increased in early grade Huntington's disease. Neurobiol. Dis. *17*, 455–461.

Guidetti, P., Bates, G.P., Graham, R.K., Hayden, M.R., Leavitt, B.R., MacDonald, M.E., Slow, E.J., Wheeler, V.C., Woodman, B., and Schwarcz, R. (2006). Elevated brain 3-hydroxykynurenine and quinolinate levels in Huntington disease mice. Neurobiol. Dis. *23*, 190–197.

Guidetti, P., Amori, L., Sapko, M.T., Okuno, E., and Schwarcz, R. (2007). Mitochondrial aspartate aminotransferase: a third kynurenate-producing enzyme in the mammalian brain. J. Neurochem. *102*, 103–111.

Gulaj, E., Pawlak, K., Bien, B., and Pawlak, D. (2010). Kynurenine and its metabolites in Alzheimer's disease patients. Adv. Med. Sci. *55*, 204–211.

Harris, J.A., Devidze, N., Halabisky, B., Lo, I., Thwin, M.T., Yu, G.Q., Bredesen, D.E., Masliah, E., and Mucke, L. (2010). Many neuronal and behavioral impairments in transgenic mouse models of Alzheimer's disease are independent of caspase cleavage of the amyloid precursor protein. J. Neurosci. *30*, 372–381.

Heyes, M.P., Saito, K., Crowley, J.S., Davis, L.E., Demitrack, M.A., Der, M., Dilling, L.A., Elia, J., Kruesi, M.J., Lackner, A., et al. (1992a). Quinolinic acid and kynurenine pathway metabolism in inflammatory and non-inflammatory neurological disease. Brain *115*, 1249–1273.

Heyes, M.P., Saito, K., and Markey, S.P. (1992b). Human macrophages convert L-tryptophan into the neurotoxin quinolinic acid. Biochem. J. *283*, 633–635.

Hilmas, C., Pereira, E.F., Alkondon, M., Rassoulpour, A., Schwarcz, R., and Albuquerque, E.X. (2001). The brain metabolite kynurenic acid inhibits alpha7 nicotinic receptor activity and increases non-alpha7 nicotinic receptor expression: physiopathological implications. J. Neurosci. *21*, 7463–7473.

Hockly, E., Cordery, P.M., Woodman, B., Mahal, A., van Dellen, A., Blakemore, C., Lewis, C.M., Hannan, A.J., and Bates, G.P. (2002). Environmental enrichment slows disease progression in R6/2 Huntington's disease mice. Ann. Neurol. *51*, 235–242.

Kessler, M., Terramani, T., Lynch, G., and Baudry, M. (1989). A glycine site associated with N-methyl-D-aspartic acid receptors: characterization and identification of a new class of antagonists. J. Neurochem. *52*, 1319–1328.

Liévens, J.C., Woodman, B., Mahal, A., Spasic-Boscovic, O., Samuel, D., Kerkerian-Le Goff, L., and Bates, G.P. (2001). Impaired glutamate uptake in the R6 Huntington's disease transgenic mice. Neurobiol. Dis. *8*, 807–821.

Mangiarini, L., Sathasivam, K., Seller, M., Cozens, B., Harper, A., Hetherington, C., Lawton, M., Trottier, Y., Lehrach, H., Davies, S.W., and Bates, G.P. (1996). Exon 1 of the HD gene with an expanded CAG repeat is sufficient to cause a progressive neurological phenotype in transgenic mice. Cell *87*, 493–506.

Masliah, E., Terry, R.D., DeTeresa, R.M., and Hansen, L.A. (1989). Immunohistochemical quantification of the synapse-related protein synaptophysin in Alzheimer disease. Neurosci. Lett. *103*, 234–239.

Masliah, E., Alford, M., DeTeresa, R., Mallory, M., and Hansen, L. (1996). Deficient glutamate transport is associated with neurodegeneration in Alzheimer's disease. Ann. Neurol. *40*, 759–766.

Miller, B.R., Dorner, J.L., Shou, M., Sari, Y., Barton, S.J., Sengelaub, D.R., Kennedy, R.T., and Rebec, G.V. (2008). Up-regulation of GLT1 expression increases glutamate uptake and attenuates the Huntington's disease phenotype in the R6/2 mouse. Neuroscience *153*, 329–337.

Misztal, M., Skangiel-Kramska, J., Niewiadomska, G., and Danysz, W. (1996). Subchronic intraventricular infusion of quinolinic acid produces working memory impairment—a model of progressive excitotoxicity. Neuropharmacology *35*, 449–458.

Moroni, F., Cozzi, A., Peruginelli, F., Carpenedo, R., and Pellegrini-Giampietro, D.E. (1999). Neuroprotective effects of kynurenine-3-hydroxylase inhibitors in models of brain ischemia. Adv. Exp. Med. Biol. *467*, 199–206.

Moroni, F., Cozzi, A., Carpendo, R., Cipriani, G., Veneroni, O., and Izzo, E. (2005). Kynurenine 3-mono-oxygenase inhibitors reduce glutamate concentration in the extracellular spaces of the basal ganglia but not in those of the cortex or hippocampus. Neuropharmacology *48*, 788–795.

Mucke, L., Masliah, E., Yu, G.Q., Mallory, M., Rockenstein, E.M., Tatsuno, G., Hu, K., Kholodenko, D., Johnson-Wood, K., and McConlogue, L. (2000). High-level neuronal expression of abeta 1-42 in wild-type human amyloid protein precursor transgenic mice: synaptotoxicity without plaque formation. J. Neurosci. *20*, 4050–4058.

Nozaki, K., and Beal, M.F. (1992). Neuroprotective effects of L-kynurenine on hypoxia-ischemia and NMDA lesions in neonatal rats. J. Cereb. Blood Flow Metab. *12*, 400–407.

Okuda, S., Nishiyama, N., Saito, H., and Katsuki, H. (1996). Hydrogen peroxide-mediated neuronal cell death induced by an endogenous neurotoxin, 3-hydroxykynurenine. Proc. Natl. Acad. Sci. USA *93*, 12553–12558.

Pellicciari, R., Rizzo, R.C., Costantino, G., Marinozzi, M., Amori, L., Guidetti, P., Wu, H.Q., and Schwarcz, R. (2006). Modulators of the kynurenine pathway of tryptophan metabolism: synthesis and preliminary biological evaluation of (S)-4-(ethylsulfonyl)benzoylalanine, a potent and selective kynurenine aminotransferase II (KAT II) inhibitor. ChemMedChem *1*, 528–531.

Perkins, M.N., and Stone, T.W. (1982). An iontophoretic investigation of the actions of convulsant kynurenines and their interaction with the endogenous excitant quinolinic acid. Brain Res. *247*, 184–187.

Rassoulpour, A., Wu, H.-Q., Ferré, S., and Schwarcz, R. (2005). Nanomolar concentrations of kynurenic acid reduce extracellular dopamine levels in the striatum. J. Neurochem. *93*, 762–765.

Rodgers, J., Stone, T.W., Barrett, M.P., Bradley, B., and Kennedy, P.G. (2009). Kynurenine pathway inhibition reduces central nervous system inflammation in a model of human African trypanosomiasis. Brain *132*, 1259–1267.

Romani, L., Zelante, T., De Luca, A., Fallarino, F., and Puccetti, P. (2008). IL-17 and therapeutic kynurenines in pathogenic inflammation to fungi. J. Immunol. *180*, 5157–5162.

Röver, S., Cesura, A.M., Huguenin, P., Kettler, R., and Szente, A. (1997). Synthesis and biochemical evaluation of N-(4-phenylthiazol-2-yl)benzenesulfonamides as high-affinity inhibitors of kynurenine 3-hydroxylase. J. Med. Chem. *40*, 4378–4385.

Sapko, M.T., Guidetti, P., Yu, P., Tagle, D.A., Pellicciari, R., and Schwarcz, R. (2006). Endogenous kynurenate controls the vulnerability of striatal neurons to quinolinate: Implications for Huntington's disease. Exp. Neurol. *197*, 31–40.

Scherzinger, E., Lurz, R., Turmaine, M., Mangiarini, L., Hollenbach, B., Hasenbank, R., Bates, G.P., Davies, S.W., Lehrach, H., and Wanker, E.E. (1997). Huntingtin-encoded polyglutamine expansions form amyloid-like protein aggregates in vitro and in vivo. Cell *90*, 549–558.

Schwarcz, R., Whetsell, W.O., Jr., and Mangano, R.M. (1983). Quinolinic acid: an endogenous metabolite that produces axon-sparing lesions in rat brain. Science *219*, 316–318.

Silva-Adaya, D., Perez-De La Cruz, V., Villeda-Hernandez, J., Carrillo-Mora, P., Gonzalez-Herrera, I.G., Garcia, E., Colin-Barenque, L., Pedraza-Chaverri, J., and Santamaria, A. (2010). Protective effect of l-kynurenine and probenecid on 6-hydroxydopamine-induced striatal toxicity in rats: Implications of modulating kynurenate as a protective strategy. Neurotoxicol. Terat. *33*, 303–312.

Simmons, D.A., Casale, M., Alcon, B., Pham, N., Narayan, N., and Lynch, G. (2007). Ferritin accumulation in dystrophic microglia is an early event in the development of Huntington's disease. Glia *55*, 1074–1084.

Stoy, N., Mackay, G.M., Forrest, C.M., Christofides, J., Egerton, M., Stone, T.W., and Darlington, L.G. (2005). Tryptophan metabolism and oxidative stress in patients with Huntington's disease. J. Neurochem. *93*, 611–623.

Wacker, J.L., Huang, S.Y., Steele, A.D., Aron, R., Lotz, G.P., Nguyen, Q., Giorgini, F., Roberson, E.D., Lindquist, S., Masliah, E., and Muchowski, P.J. (2009). Loss of Hsp70 exacerbates pathogenesis but not levels of fibrillar aggregates in a mouse model of Huntington's disease. J. Neurosci. *29*, 9104–9114.

Wang, J., Simonavicius, N., Wu, X., Swaminath, G., Reagan, J., Tian, H., and Ling, L. (2006). Kynurenic acid as a ligand for orphan G protein-coupled receptor GPR35. J. Biol. Chem. *281*, 22021–22028.

Yamamoto, M., Kiyota, T., Horiba, M., Buescher, J.L., Walsh, S.M., Gendelman, H.E., and Ikezu, T. (2007). Interferon-gamma and tumor necrosis factor-alpha regulate amyloid-beta plaque deposition and beta-secretase expression in Swedish mutant APP transgenic mice. Am. J. Pathol. *170*, 680–692.